Dynamic Progressive Buckling of Square Tubes

Chih-Cheng Yang
Department of Automation Engineering
Kao Yuan Institute of Technology
Lu-Chu, Kaohsiung, Taiwan 821, Republic of China
Assistant Professor

Abstract

The low velocity axial impact of thin-walled square tubes is taken as quasi-static and the influence of inertia forces is, therefore, ignored. The wrinkles develop progressively and the phenomenon is known as dynamic progressive buckling. In the present study, most of the aluminium tubes suffer symmetric crushing and some of the mild steel tubes suffer extensional crushing. Many crushed mild steel tubes have a mixed type of crushing which consists of type I and type II modes and a general mixed collapse mode is studied. For low velocity impact with large striking masses, the theoretical predictions for dynamic progressive axial crushing of thin-walled square tubes gives a reasonable agreement with the corresponding experimental results provided the effective crushing distance is recognized and, for mild steel, the influence of material strain rate sensitivity is retained for the dynamic behavior. However, for the cases of high velocity impact with small striking masses, the inertia effect is significant and the theoretical prediction using a quasi-static method is unsuitable.

Key words: thin-walled square tube, quasi-static , dynamic progressive buckling, general mixed collapse mode.

1. Introduction

As in the case of the experimental studies on the axial impact of thin-walled square tubes in the previous study [1,2], the crushing modes during low and high velocity impacts are different. The axial impact of thin-walled square tubes with low velocities, in which the strain distribution is uniform [3,4], is taken as quasi-static, and the influence of inertia forces is, therefore, ignored [5]. The wrinkles develop progressively and the phenomenon is known as dynamic progressive buckling. The deformation mode is the same as for static loading and is a quasi-static response, since inertia forces are neglected. However, these two types of responses are different because the influence of material strain rate sensitivity in dynamic progressive buckling is important for certain materials, even when inertia effects are not [5]. This aspect is studied theoretically.

There are many studies on the dynamic buckling of thin-walled square tubes subjected to axial loads. A theoretical analysis using the basic collapse elements developed by Hayduk and Wierzbicki [6] and Wierzbicki and Abramowicz [7] is reported by Abramowicz and Jones [8] for the progressive buckling of thin-walled square box columns subjected to axial loads, which considers the effective crushing distance, together with the influence of material strain rate sensitivity. It transpires that the four different deformation modes [8,9], are made up of one or two types of basic collapse elements shown in Figure 1, govern the behavior for different ranges of the dimensionless parameter *c/h* (*h* is wall thickness and *c* is side length of a square cross-section, see Figure 2). However, the collapse modes of a square tube in the experimental study of Reference [1,2] are not always the same with those mentioned in References [8,9]. Most of aluminium tubes have symmetric crushing and some of mild steel tubes have extensional crushing. But, many crushed mild steel tubes have mixed types which consist neither of six type I and two type II (asymmetric mode A [8]) nor of seven type I and one type II (asymmetric mode B [8]). Therefore, a general mixed collapse mode is studied. The theoretical mean dynamic crushing load is also compared with the experimental result.

2. Basic collapse elements

The behavior of dynamic progressive buckling on a square tube is often idealized as rigid-plastic since the energy absorbed elastically is usually not significant and dynamic (inertia) effects are neglected and the problem is treated as quasi-static. The material is regarded as rigid-perfectly plastic with a constant value of the flow stress σ_0. Since large plastic strains present in areas of high curvature, elastic effects can be neglected and σ_0 can be considered as an average flow stress. A kinematically admissible method of analysis is used to develop approximate theoretical predictions with two basic collapse elements [8], as shown in Figure 1. The energy absorbed in the type I basic folding element is [8]

$$E_1 = M_0\left(16I_1\frac{Hb}{h} + 2\pi c + 4I_3\frac{H^2}{b}\right), \qquad (1)$$

where $I_1 = 0.555$, $I_3 = 1.148$, H is defined in Figure 1 and b is the radius of the toroidal shell element in the kinematically admissible velocity field [7,8,10].

The energy absorbed in the type II basic folding element is also examined in Reference [8], but the consideration of an improved kinematic mechanism in Reference [9] gives

$$E_2 = M_0\left(2\pi\frac{H^2}{h} + 2\pi c + \pi H\right), \qquad (2)$$

which is slightly different to equation (2) in Reference [8].

3. Symmetric collapse mode

The idealized symmetric collapse mode, as shown in Figure 3(a), for a square tube with wall thickness h consists of four type I elements each of which absorbs the energy predicted by equation (1). The internal energy equates to the external work

$$4E_1 = 4M_0\left(16I_1\frac{Hb}{h} + 2\pi c + 4I_3\frac{H^2}{b}\right) = P_m\cdot 2H, \qquad (3)$$

where P_m is mean static crushing load and $2H$ is the initial axial separation between the locations of the plastic hinges at the top and bottom edges of a basic folding element as indicated in Figure 1. Then, equation (3) is minimized with respect to b and H [8]

$$\frac{H}{h} = 0.99\left(\frac{c}{h}\right)^{2/3} \qquad (4)$$

and

$$\frac{b}{h} = 0.72\left(\frac{c}{h}\right)^{1/3} \qquad (5)$$

to predict P_m

$$\frac{P_m}{M_0} = 38.11\left(\frac{c}{h}\right)^{1/3}, \qquad (6)$$

where $M_0 = \sigma_0 h^2/4$.

4. Extensional collapse mode

The square tube which suffered the extensional mode crushing is displayed in Figure 3(b). The extensional collapse mode consists of one layer with four type II elements shown in Figure 1. Therefore, by equating the internal energy absorption to the external work

$$4E_2 = 4M_0\left(2\pi\frac{H^2}{h} + 2\pi c + \pi H\right) = P_m\cdot 2H, \qquad (7)$$

and minimized with respect to H [9]

$$\frac{H}{h} = \left(\frac{c}{h}\right)^{1/2}, \qquad (8)$$

leads to mean static crushing load P_m [9]

$$\frac{P_m}{M_0} = 8\pi\left(\frac{c}{h}\right)^{1/2} + 2\pi. \qquad (9)$$

5. General mixed collapse mode

Figure 3(c) shows a general mixed mode of a square tube. A general mixed mode consists of n_1 type I and n_2 type II basic folding elements, as shown in Figure 1, with a total initial height $(n_1+n_2)H/2$. Thus, equating the internal energy absorption $(n_1E_1+ n_2E_2)$ to the external work $[P_m(n_1+ n_2)H/2]$ gives the mean static crushing load (P_m)

$$\frac{P_m}{M_0} = \frac{2}{n_1+n_2}\begin{bmatrix} 16n_1I_1\dfrac{b}{h} + 2(n_1+n_2)\pi\dfrac{c}{H} + \\ 4n_1I_3\dfrac{H}{b} + 2n_2\pi\dfrac{H}{h} + n_2\pi \end{bmatrix} \qquad (10)$$

when assuming that H and b are the same for the symmetric and asymmetric layers present in the general deformation mode. Equation (10) can also give the mean static crushing loads (P_m) of the four collapse modes in References [8,9] when set $(n_1 = 4, n_2 = 0)$, $(n_1 = 0, n_2 = 4)$, $(n_1 = 6, n_2 = 2)$ and $(n_1 = 7, n_2 = 1)$, respectively for symmetric, extensional, asymmetric A and asymmetric B modes. When minimizing equation (10) with b gives

$$\frac{H}{h} = \frac{4I_1}{I_3}\left(\frac{b}{h}\right)^2, \qquad (11)$$

and with respect to H gives

$$2n_1I_3\frac{1}{b} + n_2\pi\frac{1}{h} - (n_1+n_2)\pi\frac{c}{H^2} = 0. \qquad (12)$$

By substituting (11) into (12) leads to

$$n_2\left(\frac{b}{h}\right)^4 + 2n_1\frac{I_3}{\pi}\left(\frac{b}{h}\right)^3 - \frac{n_1+n_2}{16}\left(\frac{I_3}{I_1}\right)^2\frac{c}{h} = 0. \qquad (13)$$

When setting $n_1 = 4$ and $n_2 = 0$, equations (5) and (4) can be deduced from equations (13) and (11), respectively, for the symmetric mode. Also, when setting $n_1 = 0$ and $n_2 = 4$, equation (8) can be deduced from equations (11) together with (13) for the extensional mode. However, if we consider c/h in equation (13) as a variable, it is difficult to obtain an analytical solution when $n_1\cdot n_2 \neq 0$. A method of successive approximations is used to gain approximate solutions in Reference [9] for the asymmetric cases of $(n_1 = 6, n_2 = 2)$ and $(n_1 = 7, n_2 = 1)$. In order to obtain a more accurate solution of equation (13), c/h is considered as a known constant. Therefore, the last term on the left-hand side of equation (13) is a constant when n_1 and n_2 are known and the solution is

$$\frac{b}{h} = A_1\left(\frac{c}{h}\right)^{1/3}, \qquad (14)$$

where A_1 is a coefficient which depends on c/h and also varies with various sets of n_1 and n_2. Then, equation (11) is given as

$$\frac{H}{h} = A_2\left(\frac{c}{h}\right)^{2/3}, \qquad (15)$$

where

$$A_2 = \frac{4I_1}{I_3}A_1^2. \qquad (16)$$

These two coefficients, A_1 and A_2, are slightly different to those in equations (7), (8), (11) and (12) in Reference [9] for the asymmetric cases of $(n_1 = 6, n_2 = 2)$ and $(n_1 = 7, n_2 = 1)$ because $5 \le c/h \le 100$ [9].

Finally, minimization of equation (10) gives

$$\frac{P_m}{M_0} = B_1\left(\frac{c}{h}\right)^{1/3} + B_2\left(\frac{c}{h}\right)^{2/3} + B_3\pi\,, \tag{17}$$

where

$$B_1 = \frac{64n_1}{n_1+n_2} I_1 A_1 + \frac{4\pi}{A_2}\,, \tag{18}$$

$$B_2 = \frac{4n_2}{n_1+n_2}\pi A_2 \tag{19}$$

and

$$B_3 = \frac{2n_2}{n_1+n_2}\,. \tag{20}$$

6. Effective crushing distance

A simplified method for the determination of the effective crushing distance of compressed box columns is introduced in Reference [11] by using the geometry of the completely crushed basic folding mechanisms. It is shown in Reference [8] that the effective crushing distance is

$$\frac{\delta_1}{2H} = 0.73 \tag{21}$$

for the symmetric collapse mode and

$$\frac{\delta_e}{2H} = 0.77 \tag{22}$$

for the extensional and the asymmetric mixed collapse modes. It is transpires from References [7] and [11] that the differences in the crushing distance do not alter the right-hand sides of equations (1) and (2) [9]. Therefore, assuming [9]

$$\overline{P}_m\delta_1 = P_m 2H \tag{23}$$

and using equations (6) and (21) gives a dimensionless mean crushing load

$$\frac{\overline{P}_m}{M_0} = 52.20\left(\frac{c}{h}\right)^{1/3} \tag{24}$$

for a square tube with the symmetric mode of deformation [8,9]. Similarly, [9]

$$\overline{P}_m\delta_e = P_m 2H \tag{25}$$

and equations (9), (17) and (22) predict mean crushing loads [9]

$$\frac{\overline{P}_m}{M_0} = 32.64\left(\frac{c}{h}\right)^{1/2} + 8.16 \tag{26}$$

for the extensional collapse mode, and

$$\frac{\overline{P}_m}{M_0} = B_1'\left(\frac{c}{h}\right)^{1/3} + B_2'\left(\frac{c}{h}\right)^{2/3} + B_3' \tag{27}$$

for a square tube with a general mixed collapse mode, where

$$B_1' = 83.12\frac{n_1}{n_1+n_2} I_1 A_1 + 16.32\frac{1}{A_2}\,, \tag{28}$$

$$B_2' = 16.32\frac{n_2}{n_1+n_2} A_2 \tag{29}$$

and

$$B_3' = 8.16\frac{n_2}{n_1+n_2}\,. \tag{30}$$

7. Material strain rate sensitivity

For dynamic impact tests, the influence of strain rate sensitivity should be retained in the theoretical analysis for mild steel square tubes because its importance [8]. The empirical Cowper-Symonds uniaxial constitutive equation

$$\frac{\sigma_0^d}{\sigma_0^s} = 1 + \left(\frac{\dot{\varepsilon}}{D}\right)^{1/q} \tag{31}$$

is widely used to assess material strain rate effects in structures [5], where the superscripts *d* and *s* denote dynamic and static behavior, respectively. The two material constants, $D = 3\times10^7 \text{s}^{-1}$ and $q = 17$, are obtained in Reference [12] from experimental tests on specimens for the ultimate stress mild steel.

The average strain rate in an axially crushed square tubes is estimated as [8]

$$\dot{\varepsilon} = \frac{hV_m}{2b_f\delta}\,, \tag{32}$$

where δ is the effective crushing distance and V_m is the mean velocity of the striking mass during crushing [8,9]

$$V_m = \frac{V}{2}\,, \tag{33}$$

V is the initial velocity at impact. The final rolling radius b_f is associated with the toroidal deformation surface and is derived in Appendix 1 of Reference [8]. When using (4) and (15), it is shown that

$$\frac{b_f}{h} = 0.53\left(\frac{c}{h}\right)^{1/3} \tag{34}$$

and

$$\frac{b_f}{h} = A_b\left(\frac{c}{h}\right)^{1/3} \tag{35}$$

for the symmetric collapse mode and general mixed collapse mode, respectively, where $A_b = 0.53\sqrt{A_2}$.

Equation (32) together with equations (33), (4), (15), (21), (22), (34) and (35) predicts

$$\dot{\varepsilon} = 0.33\frac{V}{c} \tag{36}$$

and

$$\dot{\varepsilon} = A_s\frac{V}{c} \tag{37}$$

for the symmetric collapse mode and general mixed collapse mode, respectively, where $A_s = 0.16/A_2A_b$. It may be shown that [8,9]

$$\dot{\varepsilon} \cong 0.25\frac{V}{c} \tag{38}$$

for the extensional collapse mode.

When replacing σ_0 in equations (24), (26) and (27) (where $M_0 = \sigma_0 h^2/4$) by σ_0^d given by equation (31) if σ_Y

$\cong \sigma_u$ and equations (36)-(38), the mean dynamic crushing loads are

$$\frac{\overline{P}_m^d}{M_0} = 52.20\left[1+\left(0.33\frac{V}{cD}\right)^{1/q}\right]\left(\frac{c}{h}\right)^{1/3} \quad (39)$$

$$\frac{\overline{P}_m^d}{M_0} = \left[1+\left(0.25\frac{V}{cD}\right)^{1/q}\right]\left[32.64\left(\frac{c}{h}\right)^{1/2}+8.16\right] \quad (40)$$

$$\frac{\overline{P}_m^d}{M_0} = \left[1+\left(A_s\frac{V}{cD}\right)^{1/q}\right]\left[B_1'\left(\frac{c}{h}\right)^{1/3}+B_2'\left(\frac{c}{h}\right)^{2/3}+B_3'\right] \quad (41)$$

for the symmetric, extensional and general mixed collapse modes, respectively, and where $D = 3\times10^7 s^{-1}$ and $q = 17$ according to the material test results in Reference [12] on mild steel specimens for the ultimate stress.

8. Mean plastic flow stress σ_0

The plastic flow stress in the expression for the fully plastic moment $M_0 = \sigma_0 h^2/4$ may be defined as [9]

$$\sigma_0(\varepsilon_0) = \frac{\int_0^{\varepsilon_0}\sigma(\varepsilon)d\varepsilon}{\varepsilon_0} \quad (42)$$

to predict a more realistic value of average stresses during the crushing process. However, according to the experimental study for the static tests on square tubes, the experimental mean crushing force P_m of a mild steel tube is close to the theoretical prediction $P_{m0(UTS)}$ with $\sigma_0 = \sigma_{UTS}$ [13], but, for an aluminium tube, P_m is close to the theoretical prediction $P_{m0(0.2\%p)}$ when $\sigma_0 = \sigma_{0.2\%}$ [14]. The flow stress doesn't reach the ultimate stress when the present aluminium tube is compressed to the unstable state, instead, the flow stress reaches the 0.2% proof stress, approximately, then the tube buckles. While, when the mild steel tube is compressed to the unstable state, the flow stress has passed through the 0.2% proof stress and the maximum stress almost equals to the ultimate stress. Therefore, the mean flow stress σ_0 for aluminium square tubes is equal to the 0.2% proof stress, approximately, while for mild steel square tubes, $\sigma_0 \cong \sigma_{UTS}$. The two approximations, $\sigma_0 \cong \sigma_y$ and $\sigma_0 \cong \sigma_{UTS}$, have been used already in Reference [9].

9. Comparison between theoretical and experimental results

Some experimental results and theoretical predictions for the mean dynamic crushing loads are listed in Tables 1 and 2 for mild and aluminium specimens, respectively. The subscript LDV denotes the measurement with the aid of a laser Doppler velocimeter system. The deformation of a specimen, ΔL_{LDV}, is given by integrating the laser Doppler velocimeter signal. The limits of the integral were taken at initial impact and at the first zero velocity, and therefore, the laser Doppler velocimeter result also includes any elastic deformation of the specimen. The absorbed energy E_a is calculated from initial impact to the first zero velocity and E is the total kinetic energy. The experimental mean dynamic crushing force P_m^d and is obtained by

$$P_m^d = \frac{\int_0^{\Delta L_{LDV}} P(x)dx}{\Delta L_{LDV}}. \quad (43)$$

The theoretical prediction of the mean dynamic crushing force $\overline{P}_m^d$ is given by using Equations (39)-(41) for mild steel tubes and Equations (24), (26) and (27) for aluminium tubes.

The theoretical predictions for dynamic progressive axial crushing of thin-walled square tubes gives a reasonable agreement with the corresponding experimental results provided the effective crushing distance is recognized and, for mild steel cases, the influence of material strain rate sensitivity is retained for the dynamic behavior. The influence of material strain rate sensitivity is important for mild steel since, as displayed in Table 1, where $\overline{P}_m^{d(n)}$ is the theoretical prediction without strain rate effect which is not as accurate as the theoretical prediction with strain rate effect when compared to the experimental results. However, when increasing the impact velocity, the inertia effect becomes important and the difference between the experimental results and theoretical predictions increases although many regular wrinkles are still formed on the tubes. This phenomenon can be observed in Figures 4 and 5 for mild steel and aluminium specimens, respectively. The corresponding experimental results are listed in Tables 3 and 4 for the mild steel and aluminium specimens, respectively. The ratios of the experimental results to theoretical predictions increase as an increase of impact velocity. When the impact velocities are low with large striking masses, the ratios are close to 1, i.e. a good agreement between theoretical predictions and experimental results, except for the case with only a few regular complete wrinkles on a tube when mean crushing load is strongly influenced by the first peak load [13,14]. For high velocity impacts with small striking masses, the inertia effect is important and, in addition, the strain distribution is not uniform all over a tube [3,4], therefore the difference between experimental result and theoretical prediction by using a quasi-static method increases, as displayed in Figures 4 and 5.

As discussed in Reference [15], the transverse inertia effects should be important in general for higher velocity impact. The mode of deformation of the structure under dynamic loading may be significantly different from the quasi-static mode on account of 'inertia forces' developed within the structure by the rapid acceleration which parts of it experience during the impact. Tam and

Calladine [16] conducted more detailed experimental on a simple plate-structure and pointed out that inertia is the dominant factor in the first phase (pure compression phase) of the dynamic response to impact, while, in contrast, the second phase, in which erergy is dissipated by the rotation of plastic hinges, is more sensitive to strain-rate effects. However, according to the study on the energy-absorbing structures by Su, Yu and Reid [17], the inertia effect appears to be the dominant factor in the entire deformation, rather than only in the first phase as suggested in Reference [16], and the strain-rate effect enhances the load-carrying capacity of these types of structures during their entire dynamic deformation. The combined effects of strain-rate and inertia make the peak load much higher and the final displacement much smaller.

When the impact velocities are low with large striking masses, the ratios of the experimental results to theoretical predictions decrease with an increase of the impact velocity because the influence of the first peak load is not significant when more complete wrinkles are formed. This phenomenon also occurs in the test groups of smaller striking masses, as shown in Figures 4 and 5 for the mild steel and aluminium tubes, respectively. However, since, when increasing the impact velocity, the importance of the inertia effect increases which makes the first peak load higher, also, the complete wrinkles in the tubes of small striking mass test group are less than those of large striking mass test group when in the same levels of the striking energy, as investigated in References [1,2], the ratios for high impact velocities (small striking masses) are larger than for low impact velocities (large striking masses) and the slopes of ratio to impact velocity for the same striking mass groups tend to decrease at the higher velocities, as shown in the figures. That is, for the high velocity impacts with a same small striking mass, the influence of the first peak load on the mean dynamic crushing load is significant when the deformation is small (smaller impact velocity), while, although higher impact velocity may cause more deformation which may reduce the influence of the first peak load on the mean crushing load, the rising peak load which is caused by the inertia effect for higher velocity impact increases the mean crushing load, therefore, the ratios do not vary significantly when increasing the impact velocity with a small striking mass.

In addition, although the strain rate effect is not significant for the present aluminium tubes, except for the inertia effect, the strain-hardening effect is important for high speed impact which causes large strains in the tube [3].

10. Conclusion

The low velocity axial impact of thin-walled square tubes is taken as quasi-static and the influence of inertia forces is, therefore, ignored. The wrinkles develop progressively and the phenomenon is known as dynamic progressive buckling. In the present study, most of the aluminium tubes suffer symmetric crushing and some of the mild steel tubes suffer extensional crushing. Many crushed mild steel tubes have a mixed type of crushing which consists of type I and type II modes and a general mixed collapse mode is studied. For low velocity impact with large striking masses, the theoretical predictions for dynamic progressive axial crushing of thin-walled square tubes gives a reasonable agreement with the corresponding experimental results provided the effective crushing distance is recognized and, for mild steel, the influence of material strain rate sensitivity is retained for the dynamic behavior. However, for the cases of high velocity impact with small striking masses, the inertia effect is significant and the theoretical prediction using a quasi-static method is unsuitable.

Acknowledgement

The author wishes to thank to Dr. R. S. Birch, for his unfailing support, while Mrs. M. White, Mr. G. Swallow and Mr. J. Curran provided invaluable assistance throughout the project.

References

1. Yang, C. C., Dynamic Axial Crushing of Aluminium Square Tubes, *Proceedings of the 18th National Conference on Mechanical Engineering*, Taiwan, R.O.C., Vol. **3,** pp1033-1040, 2001.
2. Yang, C. C., Dynamic Axial Crushing of Square Mild Steel Tubes, *The 25th Conference on Theoretical and Applied Mechanics*, Taiwan, R.O.C., pp2697-2713, 2001.
3. Yang, C. C., Strain Analysis in Buckling Behavior of Square Tube Under Axial Impact, *The 7th ROC Symposium on Fracture Science*, Taiwan, ppA3-05-01~A3-05-11, R.O.C., 2002.
4. Yang, C. C., Strain Analysis in Buckling Behavior of Mild Steel Square Tubes under Axial Impact, *The 26th Conference on Theoretical and Applied Mechanics*, Taiwan, R.O.C., H001, pp1-13, 2002.
5. Jones, N., *Structural Impact*, Cambridge University Press, Cambridge, U.K., 1989.
6. Hayduk, R. J. and Wierzbicki, T., Extensional collapse modes of structural members, *Computers & Structures*, **18**(3), 447-458, 1984.
7. Wierzbicki, T. and Abramowicz, W., On the crushing mechanics of thin-walled structures, *Journal of Applied Mechanics*, **50**, 727-734, 1983.
8. Abramowicz, W. and Jones, N., Dynamic axial crushing of square tubes, *International Journal of Impact Engineering*, **2**(2), 179-208, 1984.
9. Abramowicz, W. and Jones, N., Dynamic progressive buckling of circular and square tubes, *International Journal of Impact Engineering*, **4**(4), 243-270, 1986.

10. Wierzbicki, T., Crushing behavior of plate intersections, *Structural Crashworthiness*, Eds.: Jones, N. and Wierzbicki, T., Chapter 3, 66-95, Butterworths, London, 1983.
11. Abramowicz, W., The effective crushing distance in axially compressed thin-walled metal columns, *International Journal of Impact Engineering*, **1**(3), 309-317, 1983.
12. Yang, C. C., Material Properties of Square Tube, *The 9th Fundamental Scientific Conference of Chinese Armed Forces Academy*, Taiwan, R.O.C., Vol. **1,** ppB1~11, 2002.
13. Yang, C. C. and Jones, N., Static Compression of Mild Steel Square Tubes, *Proceedings of the 16th National Conference on Mechanical Engineering*, Taiwan, R.O.C., Vol. **3,** pp51-58, 1999.
14. Yang, C. C., Static Axial Crushing of Aluminium Square Tubes, *The 77th Anniversary Conference of Chinese Military Academy*, The Chinese Military Academy, Taiwan, R.O.C., 2001.
15. Calladine, C. R. and English, R. W., Strain rate and inertia effects in the collapse of two types of energy-absorbing structure, *International Journal of Mechanical Sciences*, **26**(11/12), 689-701, 1984.
16. Tam, L. L. and Calladine, C. R., Inertia and strain-rate effects in a simple plate structure under impact loading, *International Journal of Impact Engineering*, **11**, 349-377, 1991.
17. Su, X. Y., Yu, T. X. and Reid, S. R., Inertia-sensitive impact energy-absorbing structures part II: effect of strain rate, *International Journal of Impact Engineering*, **16**(4), 673-689, 1995.

Table 1 Experimental results of mild steel square tubes with a laser Doppler velocimeter system.

specimen No	m	μ	L	ΔL_{LDV}	V_{LDV}	V_{m}	E	E_{a}	P_m^d	$\overline{P}_m^d$	$\overline{P}_m^{d(n)}$	Mode of deformation
	(kg)		(mm)	(mm)	(m/s)	(m/s)	(kJ)	(kJ)	(kN)	(kN)	(kN)	
L07	5.48	45.0	146.0	92.7	29.15	13.21	2.331	2.321	22.8	23.8	15.6	General mixed
L06	5.48	45.1	146.1	35.0	18.12	8.42	0.900	0.895	23.9	22.1	14.8	Symmetric
B06	0.90	7.3	146.1	34.0	46.21	22.17	0.964	0.945	27.3	24.2	16.2	Extensional

(n): theoretical prediction without strain rate effect by using Equations (24), (26) and (27).

Table 2 Experimental results of aluminium square tubes with a laser Doppler velocimeter system.

specimen No	m	μ	L	ΔL_{LDV}	V_{LDV}	V_{m}	E	E_{a}	P_m^d	$\overline{P}_m^d$	Mode of deformation
	(kg)		(mm)	(mm)	(m/s)	(m/s)	(kJ)	(kJ)	(kN)	(kN)	
H08	5.48	133.9	146.1	98.6	18.34	9.15	0.922	0.920	9.3	8.8	Symmetric
H13	0.90	22.2	146.1	57.7	32.69	14.32	0.483	0.476	8.3	8.6	General mixed
H16	0.40	9.9	146.1	59.0	55.86	23.35	0.630	0.616	10.4	8.8	Symmetric

Table 3. Experimental results for mild steel square tubes.

Spec. No.	μ	L (mm)	ΔL (mm)	V (m/s)	E (kJ)	P_m^d (kN)	n_I	n_{II}	
				m = 5.55kg					
C86	45.5	146.0	16.5	13.90	0.536	32.5	0	4	E
C02	45.6	146.1	30.9	17.08	0.810	26.2	8	0	S
C03	45.5	146.1	46.6	20.92	1.215	26.1	11	3	G
C04	45.5	146.1	67.3	24.25	1.631	24.2	17	3	G
C05	45.5	146.1	83.3	26.94	2.014	24.2	14	6	G
C24	46.3	146.1	118.7	31.20	2.702	22.8	14	14	G
				m = 1.87kg					
Y11	15.6	145.8	19.7	25.46	0.607	30.9	0	4	E
Y12	15.4	146.0	31.4	33.48	1.050	33.4	5	3	G
C17	15.4	146.1	45.9	37.93	1.347	29.3	2	6	G
Y13	15.4	146.0	53.7	41.38	1.604	29.9	0	12	E
C12	15.4	146.1	59.5	44.26	1.835	30.9	0	12	E
C14	15.4	146.1	65.8	45.53	1.942	29.5	6	8	G
C13	15.5	146.1	72.4	46.76	2.048	28.3	14	6	G
S4	15.4	145.8	81.9	51.35	2.469	30.1	12	8	G
C15	15.6	146.1	103.2	56.78	3.020	29.3	6	14	G
C16	15.6	146.1	110.7	60.03	3.375	30.5	9	11	G
				m = 0.95kg					
Y21	7.9	146.0	20.8	38.77	0.711	34.3	1	3	G
Y03	7.8	145.9	25.6	43.59	0.899	35.2	0	8	E
C21	7.8	146.1	30.3	46.06	1.004	33.2	3	1	G
Y22	7.9	145.9	33.7	49.96	1.181	35.1	0	8	E
C84	7.7	146.1	38.9	52.65	1.313	33.8	0	8	E
Y23	7.9	145.9	49.2	58.01	1.593	32.4	0	8	E
C22	7.8	146.1	52.8	61.78	1.807	34.3	0	8	E
Y24	7.8	145.9	61.0	65.06	2.003	32.8	0	12	E
Y25	7.8	146.0	70.2	71.61	2.427	34.6	0	12	E
C34	7.8	146.1	86.5	78.83	2.943	34.0	23	3	G
				m = 0.44kg					
Y32	3.6	145.8	27.1	70.53	1.094	40.3	0	8	E
Y33	3.6	145.8	34.4	79.80	1.401	40.7	0	8	E
S1	3.6	145.9	46.5	92.10	1.866	40.1	0	12	E
C23	3.6	146.1	55.5	94.41	1.961	35.3	4	8	G
Y35	3.7	145.9	56.4	99.21	2.165	38.4	3	9	G
C32	3.6	146.1	70.0	103.29	2.334	33.4	18	4	G
				m = 0.28kg					
Y42	2.3	146.0	24.2	84.81	0.999	41.4	0	4	E

n_I: number of type I collapse element;
n_{II}: number of type II collapse element
S: Symmetric; E: Extensional; G: General mixed

Table 4. Experimental results for aluminium square tubes.

Spec. No.	μ	L (mm)	ΔL (mm)	V (m/s)	E (kJ)	P_m^d (kN)	n_I	n_{II}	
				m = 5.55kg					
N03	136.5	146.1	22.1	8.58	0.204	9.2	4	0	S
N85	133.2	146.0	23.9	9.36	0.243	10.2	8	0	S
N75	136.9	145.7	30.4	10.06	0.281	9.2	12	0	S
N01	136.5	146.1	39.7	12.14	0.409	10.3	9	3	G
N88	137.1	145.9	55.9	13.15	0.480	8.6	16	0	S
N76	136.9	146.6	68.3	14.84	0.611	8.9	28	0	S
N02	133.1	146.1	85.5	17.12	0.813	9.5	40	0	S
N99	137.4	146.1	108.3	17.91	0.890	8.2	44	0	S
				m = 1.87kg					
G6	46.1	145.9	16.0	13.49	0.170	10.7	4	0	S
N14	46.3	146.1	22.0	16.28	0.248	11.3	4	0	S
N84	46.1	145.9	30.1	17.99	0.303	10.1	12	0	S
G2	44.9	146.0	34.7	20.70	0.401	11.6	16	0	S
N11	46.2	146.2	39.2	22.75	0.485	12.4	9	3	G
G4	44.9	146.0	48.4	24.72	0.572	11.8	12	4	G
G5	46.1	145.9	61.1	25.34	0.601	9.8	28	0	S
G3	46.1	146.0	61.2	26.64	0.664	10.9	28	0	S
N12	44.9	146.1	93.7	32.47	0.987	10.5	40	0	S
				m = 0.95kg					
N24	22.7	146.1	20.2	24.10	0.275	13.6	2	2	G
N21	23.3	146.1	44.9	33.34	0.526	11.7	20	0	S
N93	23.3	146.0	66.7	38.39	0.698	10.5	24	0	S
N22	22.7	146.1	83.6	44.68	0.945	11.3	32	0	S
N34	22.7	146.0	96.7	48.24	1.102	11.4	40	0	S
				m = 0.44kg					
N81	10.9	146.0	20.9	35.35	0.275	13.2	4	0	S
N31	10.6	146.1	29.4	41.39	0.377	12.8	12	0	S
G1	10.8	146.0	40.4	47.27	0.492	12.2	8	0	S
N95	10.8	146.0	58.2	57.29	0.718	12.3	24	0	S
N33	10.8	146.1	76.6	66.83	0.977	12.8	29	1	G
				m = 0.28kg					
N43	6.9	146.1	17.4	43.98	0.269	15.5	0	4	E
N96	6.8	146.1	30.4	55.09	0.422	13.9	6	0	S
N44	6.7	146.1	36.4	63.51	0.561	15.4	8	2	G
N42	6.8	146.1	62.0	77.02	0.825	13.3	24	2	G
				m = 0.16kg					
N52	4.0	146.1	13.2	54.20	0.242	18.3	2	2	G
N53	4.0	146.1	23.4	65.89	0.357	15.3	4	0	S
H01	4.0	146.1	29.7	73.55	0.445	15.0	12	0	S
N98	4.0	146.0	46.3	102.47	0.864	18.7	0	10	E
				m = 0.13kg					
N83	3.1	146.0	13.3	61.82	0.241	18.1	4	0	S
N64	3.1	146.1	17.2	71.67	0.324	18.8	4	0	S
N61	3.1	146.1	35.6	98.27	0.608	17.1	16	0	S
N63	3.1	146.1	59.0	121.36	0.928	15.7	24	0	S

n_I: number of type I collapse element;
n_{II}: number of type II collapse element
S: Symmetric; E: Extensional; G: General mixed

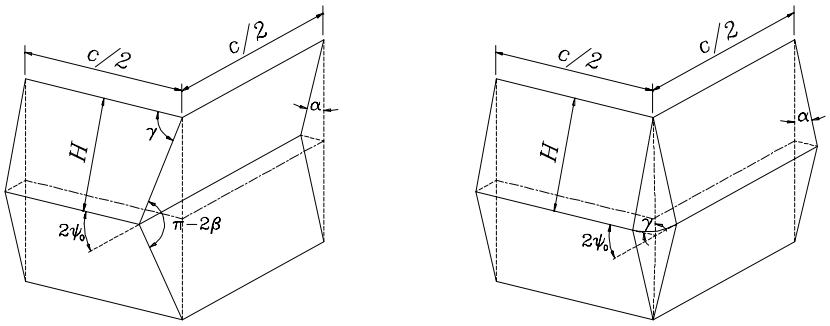

(a) (b)

Figure 1. Basic collapse elements. (a) Type I and (b) Type II

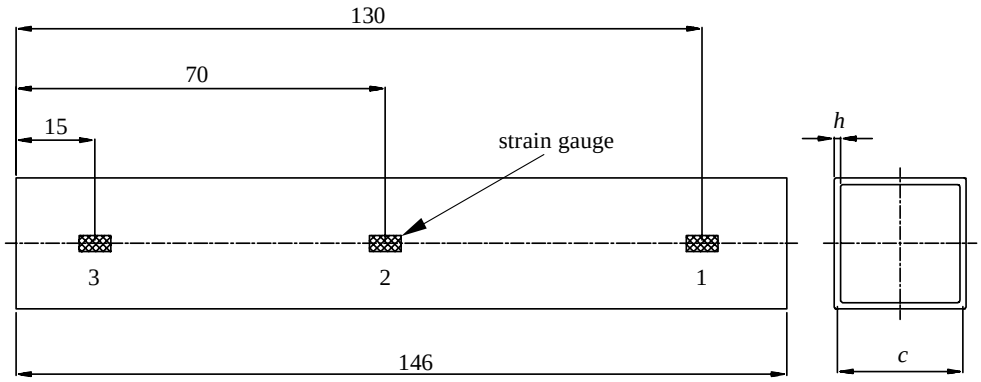

Figure 2. Geometry of a square tube specimen (in mm).

(a) (b) (c)

Figure 3. Dynamic crushing mode (dynamic progressive buckling) for a thin-walled square tube. (a) Symmetric crushing mode (N99); (b) Extensional crushing mode (Y13); (c) General mixed crushing mode (S4).

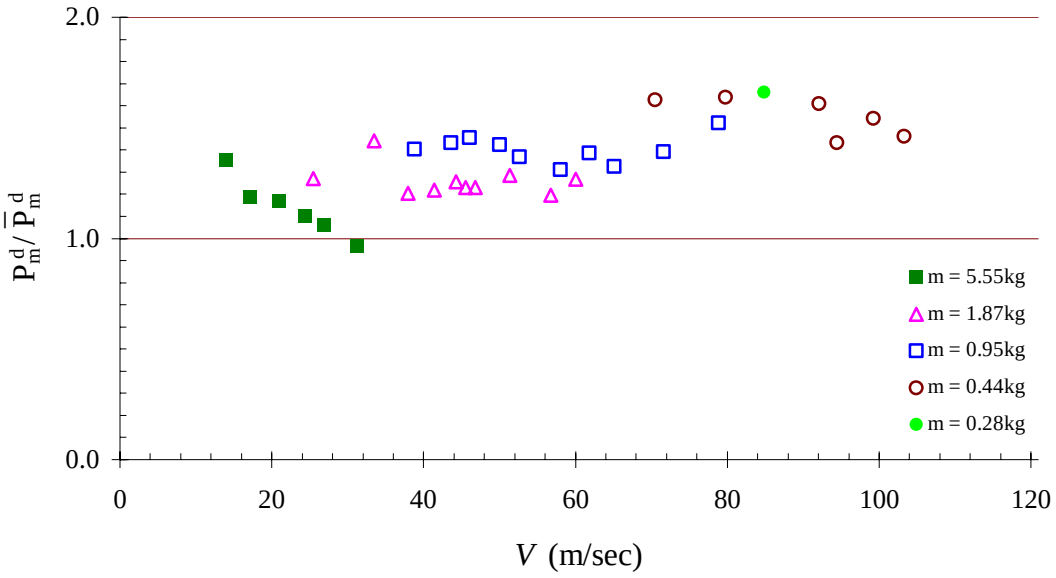

Figure 4. Ratio of experimental result to theoretical prediction versus impact velocity for mild steel tubes.

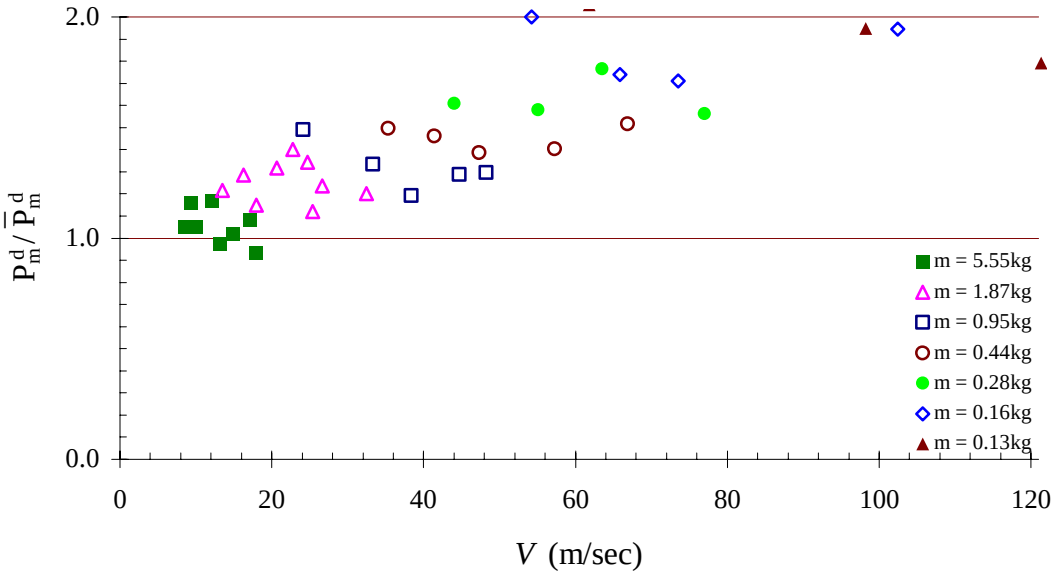

Figure 5. Ratio of experimental result to theoretical prediction versus impact velocity for aluminium tubes.

方形管之動態漸進挫曲

楊至誠
中華民國 台灣省 高雄縣
高苑技術學院 自動化工程系
助理教授

摘要

薄壁方形管的低速軸向衝擊被視為擬靜態反應、所以忽略慣性力的影響，其褶皺為漸進式地形成、因此稱為動態漸進挫曲。在此研究中、大部分的鋁管均受對稱型壓垮而一些鋼管受伸展型壓垮，多數壓垮的鋼管為型式I與型式II的混合壓垮模式、所以提出廣義混合壓垮模式。對於大撞擊質量且低速的衝擊、如果確認有效的壓垮距離及對中碳鋼而言、在動態反應中保留材料應變率敏感性的影響、則針對薄壁方管的動態漸進軸向壓垮的理論預測與相關的實驗結果相當一致。但是、對於小撞擊質量且高速的衝擊實例、其慣性效應顯著，使用擬靜態法的理論預測就不適用。

關鍵字: 薄壁方形管，擬靜態，動態漸進挫曲，廣義混合壓垮模式